

# 1 **A hydrogeomorphic dataset for characterizing catchment hydrological behavior** 2 **across the Tibetan Plateau**

3 Yuhan Guo<sup>1</sup>, Hongxing Zheng<sup>2</sup>, Yuting Yang<sup>1</sup>, Yanfang Sang<sup>3</sup>, Congcong Wen<sup>4,5</sup>

4 <sup>1</sup>State Key Laboratory of Hydrosience and Engineering, Department of Hydraulic Engineering, Tsinghua University, Beijing,  
5 100101, China

6 <sup>2</sup>CSIRO Environment, Canberra, ACT 2601, Australia

7 <sup>3</sup>Key Laboratory of Water Cycle and Related Land Surface Processes, Institute of Geographic Sciences and Natural Resources  
8 Research, CAS, Beijing, 100101, China

9 <sup>4</sup>NYUAD Center for Artificial Intelligence and Robotics, New York University Abu Dhabi, UAE

10 <sup>5</sup>NYU Tandon School of Engineering, New York University, USA

11

12 *Correspondence to:* [hongxing.zheng@csiro.au](mailto:hongxing.zheng@csiro.au)

## 13 **Abstract**

14 Hydrologic and geomorphic processes are intricately linked within the Earth system, jointly characterizing terrestrial  
15 hydrological behaviors and biogeochemical cycles across diverse temporal and spatial scales. The Tibetan Plateau provides an  
16 ideal setting for investigating the interactions between hydrological and geomorphic processes in a largely pristine natural  
17 environment. Nonetheless, the interactions remain largely unknown due to challenging physical conditions and data limitations.  
18 This study presents the inaugural version of a hydrogeomorphic dataset encompassing 18,440 catchments across the region.  
19 The dataset comprises 18 hydrogeomorphic metrics, particularly along with the width function and width function-based  
20 instantaneous unit hydrograph (WFIUH) of each catchment. We find that the peak flow of WFIUH is positively related to  
21 slope and curvature but negatively related to catchment area, perimeter, length, and circularity. The relationships of time-to-  
22 peak against the hydrogeomorphic metrics are similar to those of peak flow but in an opposite direction. Catchment  
23 concentration time shows a positive relationship with catchment size but a strong negative correlation with catchment slope.  
24 The validity of the derived WFIUH has been confirmed by its successful integration into an hourly hydrological model for  
25 simulating flash flood events. Uncertainties in the WFIUH can be attributed to the resolution of DEM and the methods  
26 employed for calculating flow velocity. The dataset is publicly available via the Zenodo portal:  
27 <https://doi.org/10.5281/zenodo.8280786> (Guo and Zheng, 2023). It can contribute to advancing our understanding of  
28 catchment hydrological behaviors and providing simple and fast routing unit hydrograph calculation for ungauged catchments  
29 in the Tibetan Plateau, and hence improve water resources management and disaster mitigation in the region and its  
30 downstream.

## 31 **1 Introduction**

32 Hydrologic and geomorphic processes are intricately linked within the Earth system, jointly characterizing terrestrial  
33 hydrological processes and biogeochemical cycles across diverse temporal and spatial scales. The interactions between these  
34 processes play a critical role in governing water flow, shaping landforms, and influencing sediment and nutrient transportation  
35 within ecosystems (Babar, 2005; Scheidegger, 1973; Sidle and Onda, 2004). The exploration of the interactions can be traced  
36 back to Horton's foundational contributions (Horton, 1945) and the classical works of Strahler (1957), Kirkby (1976) and  
37 Rodríguez-Iturbe and Valdés (1979). Since then, extensive endeavors have been undertaken in hydrology and geomorphology  
38 to investigate the hydrologic behavior of a catchment in response to its geomorphic attributes (Jenson, 1991).

39 Hydrogeomorphologic data consisting of various geomorphic attributes (e.g., slope, elevation, curvature, and catchment  
40 shape attributes) has demonstrated value in predicting hydrological behavior for ungauged basins (Esper Angillieri, 2008),  
41 mapping flood-prone zones (Lindersson et al., 2021) and determining the groundwater potential zones. On top of the  
42 morphologic or topographic metrics describing catchment properties, the geomorphologic instantaneous unit hydrograph  
43 (GIUH) introduced by Rodríguez-Iturbe and Valdes (1979) is of utmost interest for hydrologists to derive hydrograph in the  
44 absence of hydrologic data (Bhaskar et al., 1997; Jain et al., 2000; Nasri et al., 2004; Nowicka and Soczynska, 1989; Kumar  
45 et al., 2007). The concept of GIUH was extended by Gupta et al. (1980) to theoretically deduce the unit hydrograph based on  
46 geomorphology, topographic parameters, and hydrographic parameters. The GIUH assumes that the probability distribution  
47 of the water droplet travel time is exponential, which however lacks practical physical meaning (Gupta and Waymire, 1983;  
48 Kirshen and Bras, 1983; Rinaldo et al., 1991). The assumption is arguable and it is also challenging to determine flow velocity  
49 while deriving GIUH (Rodríguez-Iturbe and Valdes, 1979; Troutman and Karlinger, 1985). An alternative geomorphology-  
50 based unit hydrograph is based on the geomorphic width function (Kirkby, 1976). The width function is commonly considered  
51 as one of the most important geomorphologic and hydrologic features quantifying the influence of the river network on  
52 catchment hydrologic processes (Mesa and Mifflin, 1986; Naden, 1992), which determines the shape of the instantaneous unit  
53 hydrograph (Botter and Rinaldo, 2003). Franchini and O'Connell (1996) compared WFIUH against GIUH and suggested that  
54 WFIUH is more physically consistent and more practical.

55 The Tibetan Plateau is known as the water tower of Asia, supplying water to almost 2 billion people (Yao et al., 2012; Li  
56 et al., 2022; Mtamba et al., 2015). Hydrogeomorphic characteristics of catchments within the Tibetan Plateau are unique and  
57 with little human intervention (Yao et al., 2022; Mölg et al., 2014). The geographical uniqueness of the Tibetan Plateau  
58 provides ideal opportunities to explore the interactions between hydrologic and geomorphic processes. However,  
59 hydrogeomorphic data of catchments across the Tibetan Plateau are still limited for a systematic investigation of the  
60 hydrogeomorphic process in the region. Particularly, the Tibetan Plateau is experiencing more extreme precipitation events  
61 and floods (Ge et al., 2019; Yang et al., 2022), which makes it imperative to develop a comprehensive hydrogeomorphic  
62 dataset to inform flood modeling and adaptive watershed management.

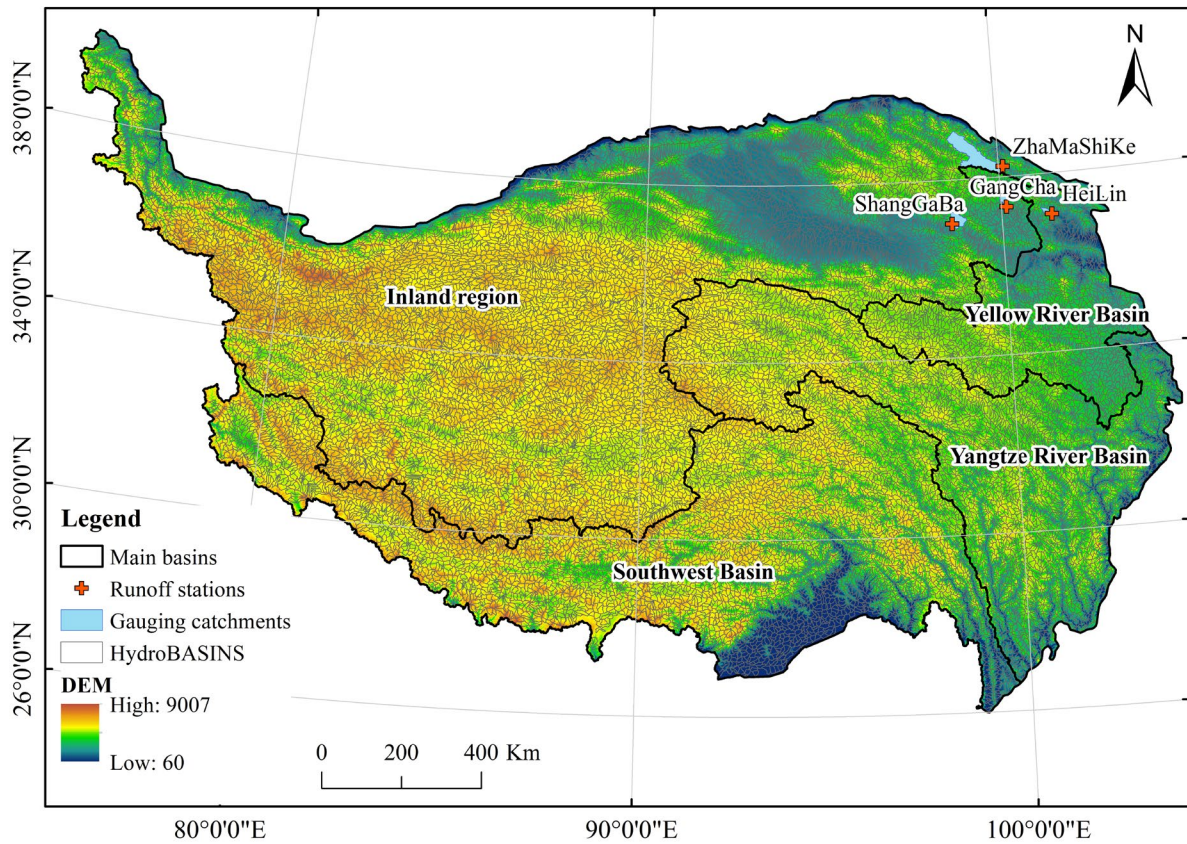
63 This research aims to provide an inaugural version of the hydrogeomorphic dataset for catchments over the Tibetan  
64 Plateau. The dataset includes 18 hydrogeomorphic measurements of 18440 catchments within the plateau, which are derived  
65 from a high-resolution digital elevation model (DEM) or compiled from existing products. Most importantly and uniquely, the  
66 research provides the first dataset of WFIUH for each catchment, which can be used to investigate the spatial heterogeneity of  
67 hydrological behavior across the Tibetan Plateau. The derived WFIUH are tested and validated as applied to flood modeling  
68 for gauged catchments. This dataset is expected to contribute to a better understanding of hydrogeomorphic processes and to  
69 facilitate hydrological modeling of catchments across the Tibetan Plateau.

## 70 **2 Study area and data**

71 The Tibetan Plateau (TP) is situated between 26° to 40°N and 73° to 105°E and has a mean elevation of more than 4500  
72 meters, occupying about  $2.5 \times 10^6$  km<sup>2</sup>. TP is the highest and most extensive highland in the world. In addition to having the  
73 largest cryospheric extent outside the polar region, the TP also serves as the source region for all major rivers in Asia.  
74 Consequently, it has been widely acknowledged as the driving force behind both regional and global environmental change  
75 (Kang et al., 2010). The Mekong River, the Yellow River, the Yangtze River, the Yarlung Tsampo (Brahmaputra), the Indus  
76 and the Karnali all originate on the Tibetan plateau and support hundreds of millions of people downstream. Due to the harsh  
77 and complex natural environment, the Tibetan Plateau is a typical ungauged area in China. Within the boundary of China, the  
78 Tibetan Plateau can be roughly divided into several basins, namely the Inland region basin, the Yellow River basin, the Yangtze  
79 River basin, and the Southwest basin (Figure 1).

80 In this study, the hydrogeomorphic dataset we developed covers 18440 catchments across the Tibetan Plateau. The  
81 boundaries of the catchments are determined according to the HydroBASINS dataset, where the 12<sup>th</sup> level catchments are  
82 considered (<https://www.hydrosheds.org/products/hydrobasins>). In deriving the width function for each catchment from the  
83 digital elevation model (DEM), it needs to produce the flow direction raster map first. The Tibetan Plateau has numerous  
84 endorheic basins (mainly in the inland region in Figure 1), and the algorithms applied to determine flow directions of endorheic  
85 and exorheic basins can be slightly different (e.g., Prusevich et al. (2022)). As this study does not focus on the algorithms  
86 determining flow direction but mainly on generating the WFIUH for flash flood modeling, we use the flow direction raster  
87 map from HydroSHEDS (<https://www.hydrosheds.org/hydrosheds-core-downloads>), which bases on DEM from NASA's  
88 Shuttle Radar Topography Mission (SRTM) with spatial resolution around 90m (Lehner et al., 2008).

89 Land cover data product FROM-GLC (Finer Resolution Observation and Monitoring-Global Land Cover) released  
90 by Peng Gong et al. (2019) is used in this study to estimate the Manning coefficient in calculating flow velocity. The  
91 spatial resolution of the land cover data is 10m. It is resampled by the bilinear approach to be consistent with the flow  
92 direction map. For hydrological modeling validity, hourly rainfall and streamflow data of 4 hydrological stations are  
93 obtained from China's Annual Hydrological Report. Boundaries of the 18440 catchments and locations of the hydrological  
94 stations are shown in Figure 1.



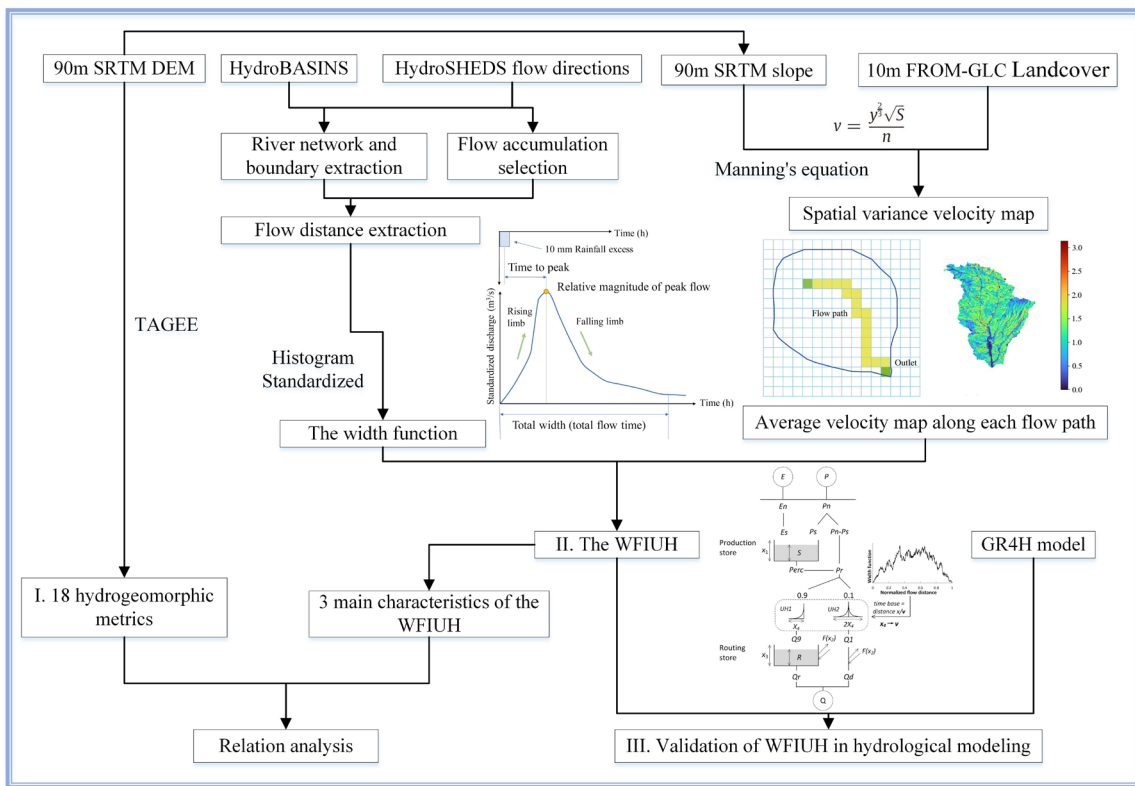
95

96 **Figure 1** Elevation and boundaries of 18440 HydroBASINS catchments across the Tibetan Plateau

97 **3 Methods**

98 The overall framework for producing the hydrogeomorphic dataset for catchments over the Tibetan Plateau is shown in  
 99 Figure 2. The framework mainly consists of three procedures, i.e., extracting critical hydrogeomorphic metrics from DEM or  
 100 existing data products, deriving width function for catchments based on terrain analysis, and generating WFIUH for all  
 101 catchments. The derived WFIUH is then tested by incorporating it into a hydrological model to simulate hydrological processes  
 102 at a catchment scale.

103



104

105 **Figure 2 Framework of developing catchment-scale hydrogeomorphic dataset of the Tibetan Plateau**

106 **3.1 Catchment-scale hydrogeomorphic metrics**

107 In this dataset, 18 hydrogeomorphic metrics at a catchment scale are retrieved from DEM or compiled from existing  
 108 datasets. The hydrogeomorphic metrics are closely related to hydrologic and geomorphic processes for the catchments,  
 109 including area, consisting of area, the longitude of centroid, latitude of centroid, mean elevation, slope, aspect, northness,  
 110 eastness, perimeter, catchment length, catchment width, elongation, circularity index, form factor, shape index, Gaussian  
 111 curvature, hillshade, horizontal curvature and vertical curvature. Definitions of each metric are shown in Table 1.

112 Several topographic and geomorphic attributes are gained from a package called Terrain Analysis in Google Earth Engine  
 113 (TAGEE) (Safanelli et al., 2020) using Google Earth Engine platforms. The curvature shows the complexity of the undulation  
 114 of the ground and it is a quantitative measure of curvature degree and change-point on the terrain surface. The horizontal  
 115 curvature indicates the degree of curvature and change of the surface along the horizontal direction, which could affect the  
 116 convergence and dispersion of water flow. The vertical curvature is the degree of elevation change along the maximum slope  
 117 of the ground slope, which could affect the speed of water flow, resulting in different erosion or accumulation rates. Mean  
 118 curvature and the Gaussian curvature both characterize the comprehensive curvature features. According to Safanelli et al.  
 119 (2020), Northness and Eastness can be derived from the aspect. The aspect and derived products, such as Northness and  
 120 Eastness attributes, can be linked to the potential solar irradiation on terrain. Mathematical expressions of these metrics listed

121 in Table 1 can be referred to Florinsky (2016). It is worth noting that the shape index (SI) is a continuous numerical form of  
 122 Gaussian landform classification proposed by Koenderink and Van Doorn (1992). The range of the shape index is -1 to 1.  
 123 When the value is negative, the surface is concave, and if the value is positive, the surface is convex. When the absolute value  
 124 of the shape index is within 0.5-1.0, the surface is elliptical. When the absolute value of the shape index is within 0-0.5, the  
 125 surface is hyperbolic. The shape index expression is as follows:

$$126 \quad SI = \frac{2}{\pi} \arctan \frac{H}{\sqrt{H^2 - K}} \quad (1)$$

127 In the formula, H and K are parameters used to characterize the shape of the surface (such as ridge or valley, convex or  
 128 concave). For illumination of the datasets, the expressions of circularity index (CI), form factor (Rf), elongation ratio (Re) and  
 129 are presented respectively herein:

$$130 \quad CI = \frac{A_{\text{catchment}}}{A_{\text{circle}}} \quad (2)$$

$$131 \quad R_f = \frac{A_{\text{catchment}}}{L_{\text{catchment}}^2} \quad (3)$$

$$132 \quad R_e = \frac{L_{\text{circle}}}{L_{\text{catchment}}} \quad (4)$$

133 where,  $A_{\text{catchment}}$ ,  $L_{\text{catchment}}$  are the area and length of a catchment.  $A_{\text{circle}}$  is the area of a circle whose perimeter equals  
 134 the watershed's perimeter.  $L_{\text{circle}}$  is the diameter of a circle that equals the catchment area. The circularity index represents  
 135 the ratio of the catchment area to the area of a circle with an equivalent perimeter. It ranges between 0 and 1. The catchment  
 136 is closer to a circular shape for a higher CI value. The Form factor is the ratio of catchment area to squared catchment length.  
 137 A higher Rf indicates a closer fan-shaped catchment. The Elongation ratio is the ratio of  $L_{\text{circle}}$  to catchment length. A smaller  
 138 value of Re reflects a more elongated catchment.

139 Metrics such as area, perimeter, catchment length, catchment width, elongation ratio, circularity index, and form factor are  
 140 retrieved from HydroBASINS sub-catchment shapes. The elevation and slope metrics are derived from SRTM DEM with a  
 141 spatial resolution of around 90m. Before retrieving the metrics for the Tibetan Plateau domain, all the maps have been  
 142 reprojected to the same coordination system.

143 **Table 1 Descriptions of 18 hydrogeomorphic metrics provided in TPHGD dataset**

Metrics	Descriptions	Units
Area	Area of catchment	km <sup>2</sup>
Perimeter	Perimeter of catchment	km
Catchment length	Straight distance from the outlet to the farthest point in a catchment	km
Catchment width	The narrowest distance perpendicular to the line between the outlet and the farthest point	km
Elevation	The mean elevation of the catchment	meter
Slope	Mean slope of the catchment	degree
Aspect	Compass direction	degree

Northness	Degree to north	N/A
Eastness	Degree to east	N/A
Circularity index	see formula 2	N/A
Form factor	see formula 3	N/A
Elongation ratio	see formula 4	N/A
Shape index	The continuous form of Gaussian landform classification, see formula 1	N/A
Hillshade	Brightness of illuminated terrain	N/A
Horizontal curvature	Curvature tangent to the contour line	meter
Vertical curvature	Curvature tangent to slope line	meter
Gaussian curvature	Product of maximal and minimal curvatures	meter
Mean curvature	Mean of horizontal and vertical curvatures	meter

144

### 145 3.2 Width function from DEM

146 The width function (WF) of a catchment is more informative than a single hydrogeomorphic metric in reflecting runoff  
 147 response to catchment landforms. The width function is defined as the probability measure at a given distance  $x$  to the outlet  
 148 of the  $i_{th}$  link measured along with the river network (Rinaldo et al., 1995). With the assumption that every water drop in the  
 149 channel network travels to the outlet at the same velocity, mathematically, the width function  $W(x)$  is expressed:

$$150 \quad W(x) = \sum_{i=1}^n b(x; x_i^u, x_i^d) \quad (5)$$

151 where  $n$  is the number of links in the network,  $x_i^u$  and  $x_i^d$  are the distances of the upstream and downstream ends of link  $i$  from  
 152 the outlet, and the function  $b(x)$  is expressed as:

$$153 \quad b(x; x_i^u, x_i^d) = \begin{cases} 1, & x_i^d \leq x < x_i^u \\ 0, & \text{otherwise} \end{cases} \quad (6)$$

154 Integrated along the longest flow path, the relationship between the catchment area and the width function can then be  
 155 expressed as (Moussa, 2008):

$$156 \quad Area = \int_0^{L_{max}} W(x) dx \quad (7)$$

157 Therefore, for comparison among different catchments, the width function can be normalized as:

$$158 \quad W'(x^*) = W(x)/Area, \text{ with } x^* = x/L_{max} \quad (8)$$

159 In this study, we develop the width function for each catchment based on the flow direction map from HydroSHEDS by  
 160 using the *pysheds* package in Python (<https://github.com/mdbartos/pysheds>). Given the flow direction map, catchment  
 161 delineation and river network extraction proceeded after the implementation of flow accumulation. The threshold of flow  
 162 accumulation is set to be the 96<sup>th</sup> percentile of the total accumulation as an easy and efficient way compared with other more  
 163 complex methods (Passalacqua et al., 2010). Based on the derived river network, the flow distance of each DEM grid is  
 164 computed and the width function is estimated as the histogram of the catchment area (represented by the number of grids)  
 165 against flow distance.

### 166 3.3 Width function-based instantaneous unit hydrograph

167 The width function is closely related to the development of a geomorphic instantaneous unit hydrograph (Singh et al.,  
168 2014). The WF-based IUH (i.e., WFIUH) is the combination of the WF with any possible linear routing scheme. If only river  
169 network routing is taken into account, the convection-diffusion equation can be applied to calculate the WFIUH after stream  
170 network ordering (Franchini and Oconnell, 1996). The expression form of WFIUH becomes the following form:

$$171 \quad WFIUH(t) = \int_0^{L_{max}} f_x(t)W(x)dx \quad (9)$$

172 where,  $f_x(t)$  represents the flow time distribution at the distance  $x$  along the river network in a watershed and  $W(x)$  is the  
173 width function.  $L_{max}$  is the largest length of the stream network.

174 Equation 9 ignores hillslope routing within a catchment. The hillslope routing however could be a critical process in  
175 determining runoff response to rainfall and shaping the IUH (Saco and Kumar, 2004). With the consideration of the effects of  
176 hillslope routing, it is proposed to combine the spatial distribution of flow velocity and the width function to derive WFIUH  
177 (Grimaldi et al. (2010), which is adopted in this study. Four approaches are commonly used to calculate flow velocity (Grimaldi  
178 et al., 2010), including Darcy–Weisbach’s formula (Katz et al., 1995), Manning’s formula, the Soil Conservation Service (SCS)  
179 formula (Haan et al., 1994), and the uniform flow formula (Maidment et al. (1996). Making use of a remotely sensed land  
180 cover dataset, we herein adopt Manning’s formula in our calculation, which is expressed as:

$$181 \quad v = \frac{v^{\frac{2}{3}}\sqrt{S}}{n} \quad (10)$$

182 where,  $n$  is Manning’s roughness coefficient that is related to the land cover type of catchments, and its unit is  $m^{-\frac{1}{3}}s$ .

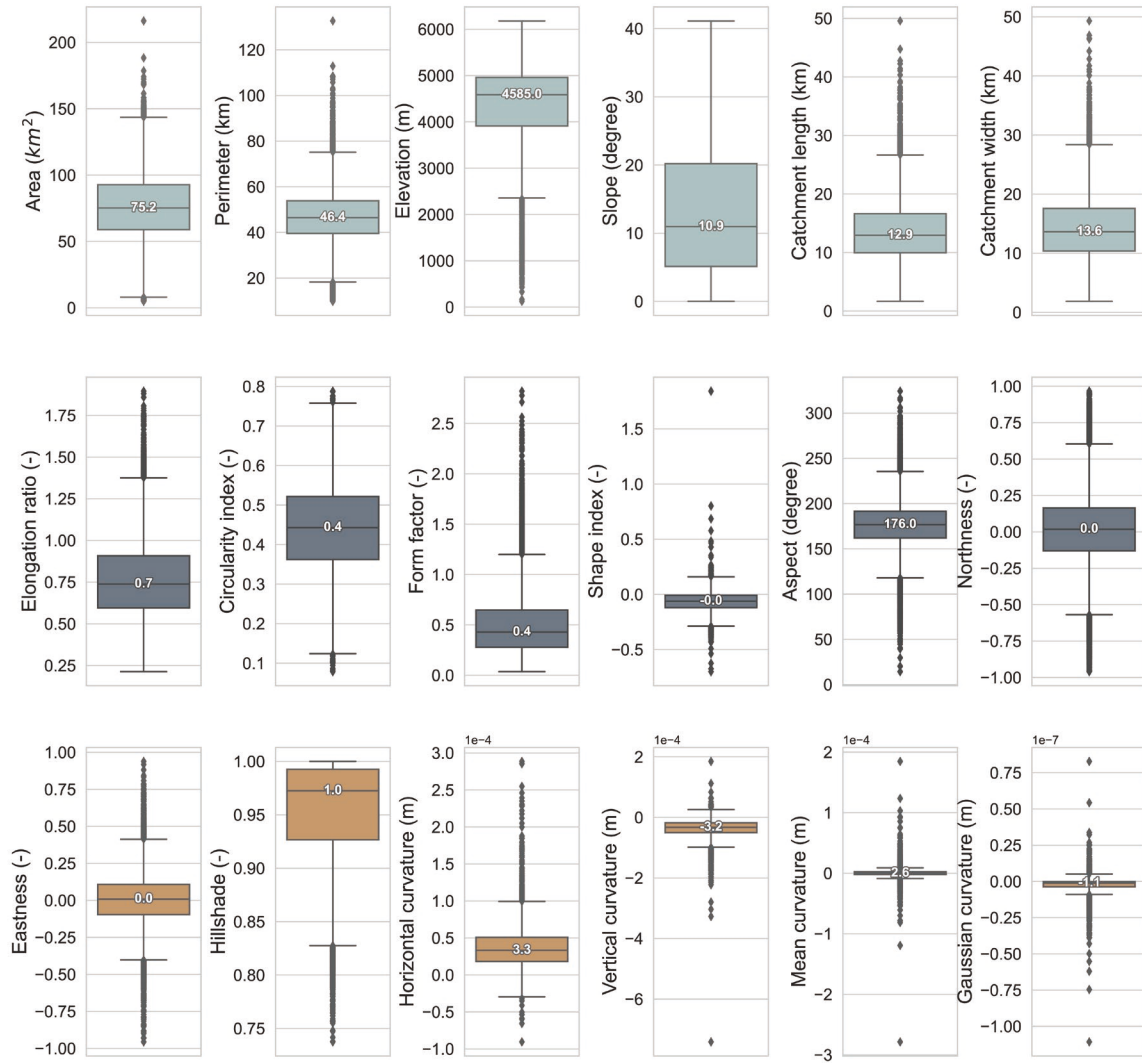
183 To calculate the velocity, as shown in Figure 2, a spatial map of the slope for each catchment is produced based on DEM  
184 from SRTM. The 10m FROM-GLC landcover data is then resampled to 90m resolution to match with that of DEM. Manning’s  
185 roughness  $n$  for each 90m grid was assigned according to the look-up table of land cover type against roughness (Table S1 in  
186 Supplementary).

## 187 4 Results

### 188 4.1 Spatial distribution of hydrogeomorphic characteristics

189 Eighteen hydrogeomorphic metrics of 18440 catchments across the Tibetan Plateau are provided in our dataset (TPHGD).  
190 Metrics of a small portion of catchments (<1%) are missing due to spatial mismatch or data quality. Figure 3 presents a  
191 statistical summary of the metrics, while Figure 4 shows spatial patterns of the metrics across the Tibetan Plateau. As shown  
192 in Figure 3, the area of the 18440 catchments ranges between 4.8 km<sup>2</sup> and 216 km<sup>2</sup>, with the perimeter that varies from 9.8 km  
193 to 132.7 km and catchment mean elevation between 123.8m to 6180.9m. Most of the catchments are located between 2200m  
194 and 6100m. Catchments with higher elevations are in the western and central parts of the TP. Catchments in the western and

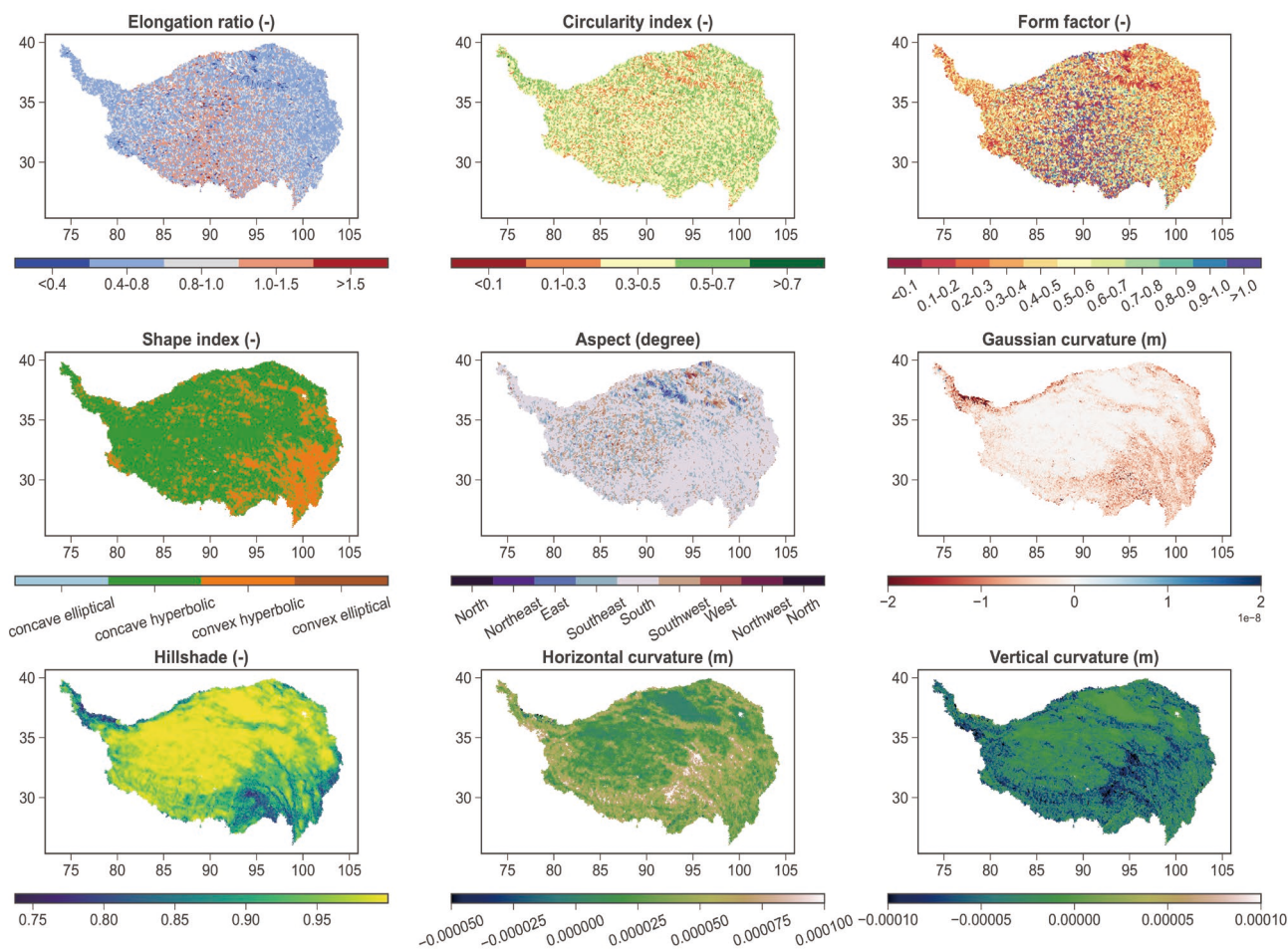
195 southeast TP are steeper than other catchments in the TP. Catchment length and width are similar in their statistical distribution  
 196 (Figure 3), both largely between 1-30km.



197  
 198 **Figure 3 Statistical summaries of 18 hydrogeomorphic metrics for 18440 catchments across the Tibetan Plateau.**

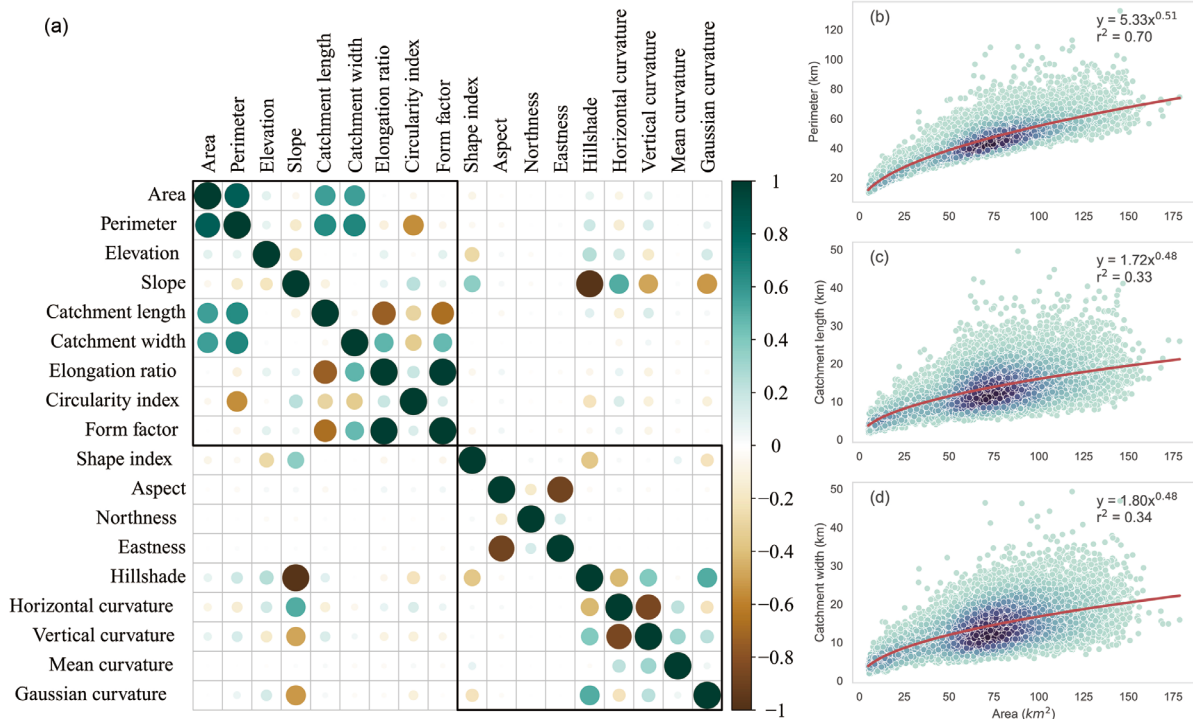
199 Ranges of the elongation ratio, circularity index, and form factor of the catchments are 0.2-1.9, 0.08-0.79, and 0.04-2.82  
 200 respectively. Around three-quarters of the catchments have an elongation ratio lower than 1, which means the majority of  
 201 catchments tend to be elongated. Catchments in central TP are more elongated ( $Re > 1.0$ ) and are with a pinnate river network  
 202 ( $Rf > 1.0$ ). Catchments located in western and eastern TP are less elongated and more fan-shaped (Figure 4). Most catchments  
 203 show concave hyperbolic land surface, with a shape index between -0.5 and 0, except for catchments located in the southeast  
 204 TP. Most catchment aspects are between 150 and 200 degrees with their northness and eastness ranging between -0.25-0.25

205 and -0.5-0.5 respectively. This reveals that most catchments in TP face southwest, south, or southeast. The hillshade of most  
 206 catchments is above 0.9 (Figure 3). Catchments in southeast TP have lower hillshade, suggesting that they are in the alpine  
 207 and valley areas with a higher shading effect. The curvature of a catchment affects the movement of water, sediment and  
 208 biogeochemical matters. In addition to the horizontal and vertical curvatures, the Gaussian and mean curvatures for each  
 209 catchment are recorded in our dataset as well. The median horizontal and vertical curvatures of all the TP catchments are  
 210 around  $0.33 \times 10^{-3}$  m and  $-0.32 \times 10^{-3}$  m respectively. Medians of mean and Gaussian curvature are  $0.26 \times 10^{-3}$  m and  $-0.11 \times 10^{-6}$   
 211 m respectively. It is worth noting that the curvature metrics in our dataset represent that at a catchment scale, which are averages  
 212 of each grid cell within the catchment. Hence, catchments with less curvature suggest a greater extent of flat or plain terrain  
 213 within the catchment.  
 214



215  
 216 **Figure 4 Spatial patterns of hydrogeomorphic metrics across the Tibet Plateau**

217 Figure 5 shows correlations among the 18 metrics. Catchment area ( $A_c$ ) is found significantly correlated with catchment  
 218 length ( $L_c$ ), width ( $L_w$ ), and perimeter ( $P_c$ ), and could be represented by the power law (Figure 5(b), (c), (d)). The relationship  
 219 between  $A_c$  and  $L_c$  largely follows Hack's law (Rigon et al., 1996; Sassolas-Serrayet et al., 2018), which suggests a power  
 220 law between the length of the river channel and the drainage area. The catchment perimeter is negatively correlated with the  
 221 circularity index (with a correlation coefficient  $r=-0.55$ ). Elongation ratio, circularity index, and form factor are highly related  
 222 to catchment length, catchment width, and perimeter as can be expected according to Eqs.2-4. The form factor and the  
 223 elongation ratio are highly related ( $r=0.98$ ). This may indicate that the elongation ratio and form index represent similar shape  
 224 information of a catchment. The slope of the catchments is correlated negatively with hillshade ( $r=-0.97$ ), vertical curvature  
 225 ( $r=-0.49$ ) and Gaussian curvature ( $r=-0.53$ ), but positively with shape index ( $r=0.36$ ) and horizontal curvature ( $r=0.52$ ). There  
 226 is no significant correlation between catchment slope and elevation with a correlation coefficient of no more than  $\pm 0.3$ .



227  
 228 **Figure 5 Correlation between the 18 hydrogeomorphic metrics (left) and relationships between catchment area against catchment**  
 229 **length, width and perimeter (right).**

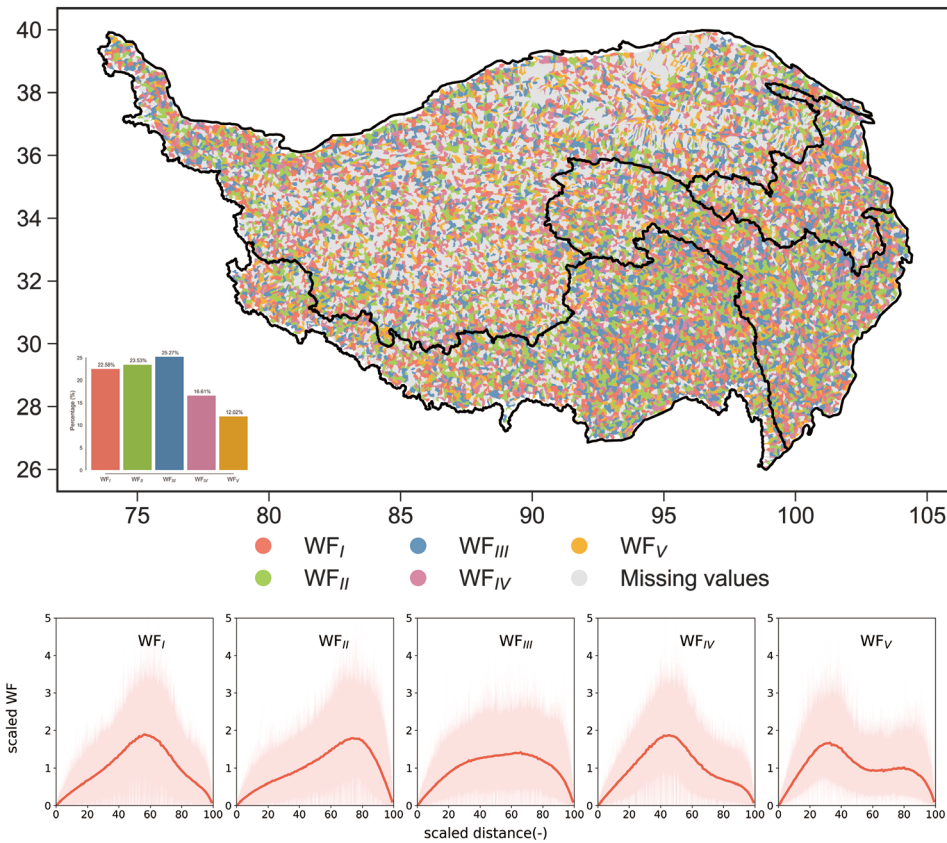
#### 230 4.2 Classification of catchment's width function

231 The width function of a catchment is a comprehensive curve reflecting the effects of landform on hydrological behavior  
 232 and is used to develop the instantaneous unit hydrograph for catchments across the TP. In TPHGD, normalized width functions  
 233 of 13,456 out of the 18,440 catchments are presented since it is less meaningful to derive the width function of a catchment

234 with a relatively smaller area. The normalized width functions of the 13,456 catchments across the TP are grouped into five  
235 types by using the K-means unsupervised clustering approach and the Gap Statistic method.

236 Shapes of the five types of width functions are shown in Figure 6. The first two types of width function both have a  
237 notable peak value in the curve (i.e., area proportion against distance to catchment outlet). However, the  $WF_I$  is peak-centered  
238 while  $WF_{II}$  is peak-skewed. The shape of catchments characterized by these two types of width functions is typically elongated,  
239 with tributaries predominantly located in the upstream areas, resulting in relatively lengthy routing pathways. The third type  
240 of the width function ( $WF_{III}$ ) is largely uniform-like without notable peaks. This width function type is often observed in  
241 catchments with larger overall areas or with a relatively consistent density of river networks extending from upstream to  
242 downstream. The fourth ( $WF_{IV}$ ) and fifth ( $WF_V$ ) types of width function are with dual peaks. The main difference between  
243 them is that the first peak in  $WF_{IV}$  is dominant, while the two peaks in  $WF_V$  are much closer values. Catchments with  $WF_{IV}$  or  
244  $WF_V$  approximately are parallel river systems, having more tributaries converging separately to catchment outlets than other  
245 catchments.

246 For the 13,456 catchments across TP, the proportion of catchments with a specific width function type are 22.58% ( $WF_I$ ),  
247 23.53% ( $WF_{II}$ ), 25.27% ( $WF_{III}$ ), 16.61% ( $WF_{IV}$ ) and 12.02% ( $WF_V$ ) respectively. As shown in Figure 6, however, there is no  
248 clear spatial pattern of the width function across the TP. The spatial distribution characteristics of the width function are  
249 relatively random, and the obvious spatial aggregation characteristics of different classification width functions cannot be  
250 found in our dataset.



251

252 **Figure 6 Typical width functions (bottom) and their spatial distribution across the Tibetan Plateau (top). At the bottom, the pink**  
 253 **background indicates ranges of width function from the catchments subset of that type, while the red curve represents the median**  
 254 **of the corresponding catchment subset.**

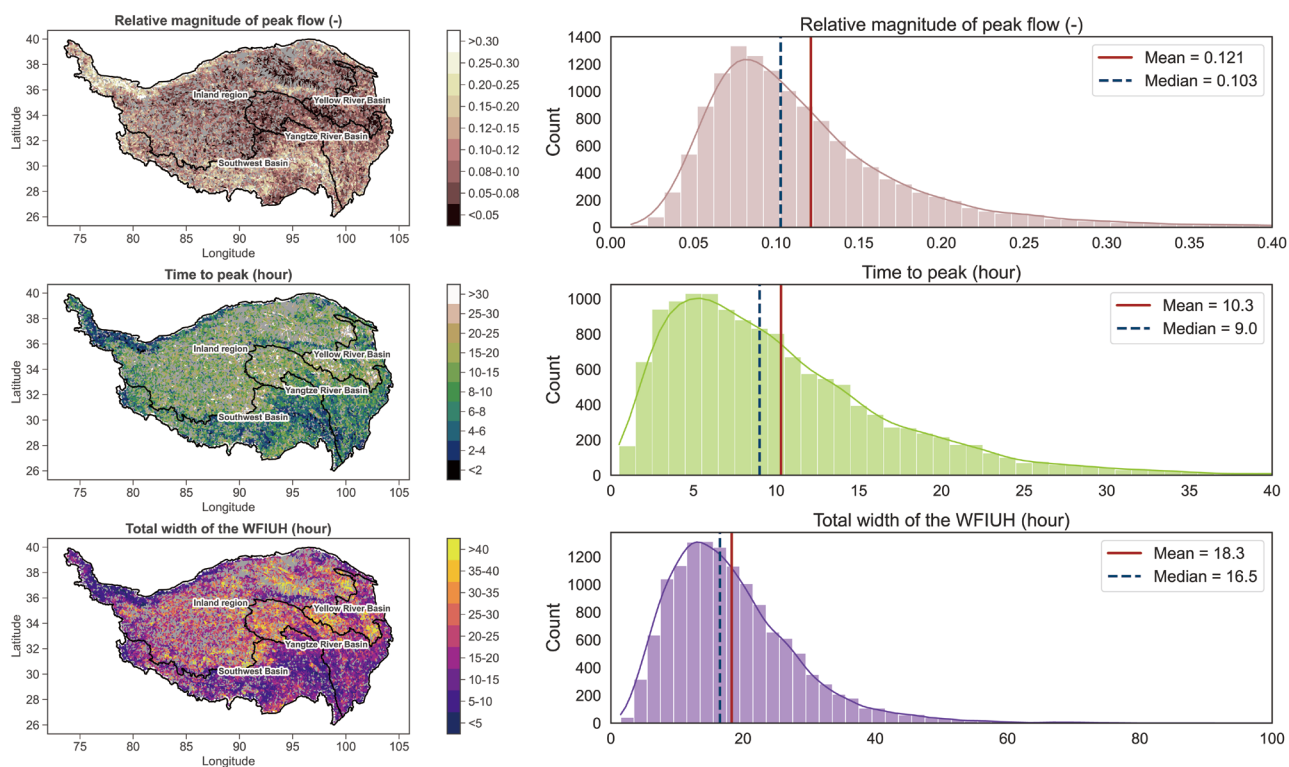
### 255 4.3 WFIUH of catchments across the Tibetan Plateau

256 Based on the catchments' width function, instantaneous unit hydrographs for each of the 13,456 catchments across the  
 257 TP are derived and presented in the TPHGD dataset, together with flow velocity estimated by Manning's approach for each  
 258 grid cell. The time interval of the derived WFIUH is 30 minutes. There are some catchments located in the eastern Continental  
 259 basin whose WFIUH cannot be extracted due to large irrigation areas and canals. Herein, characteristics of the WFIUH  
 260 indicated by peak flow magnitude ( $Q_p$ ), time to peak ( $T_p$ ) and concentration time ( $T_c$ , i.e., width of time base in WFIUH) for  
 261 catchments across the TP are investigated. Their relationships with the 18 geomorphic metrics are also examined. The box plot  
 262 of the relative magnitude of peak flow, time to peak, and the total width of the WFIUH and the spatial pattern of the three  
 263 variables is demonstrated in Figure 7. This information can reveal the distribution features of the WFIUH of 13456 catchments  
 264 in the Tibetan Plateau, which may be valuable for flood risk decision-making and management in this region.

265 As shown in Figure 7, the relative magnitude of peak flow for most catchments ranges from 0.05 to 0.15, with mean and  
 266 median are 0.121 and 0.103 respectively. The smaller relative magnitude of the peak flow value represents a more uniform

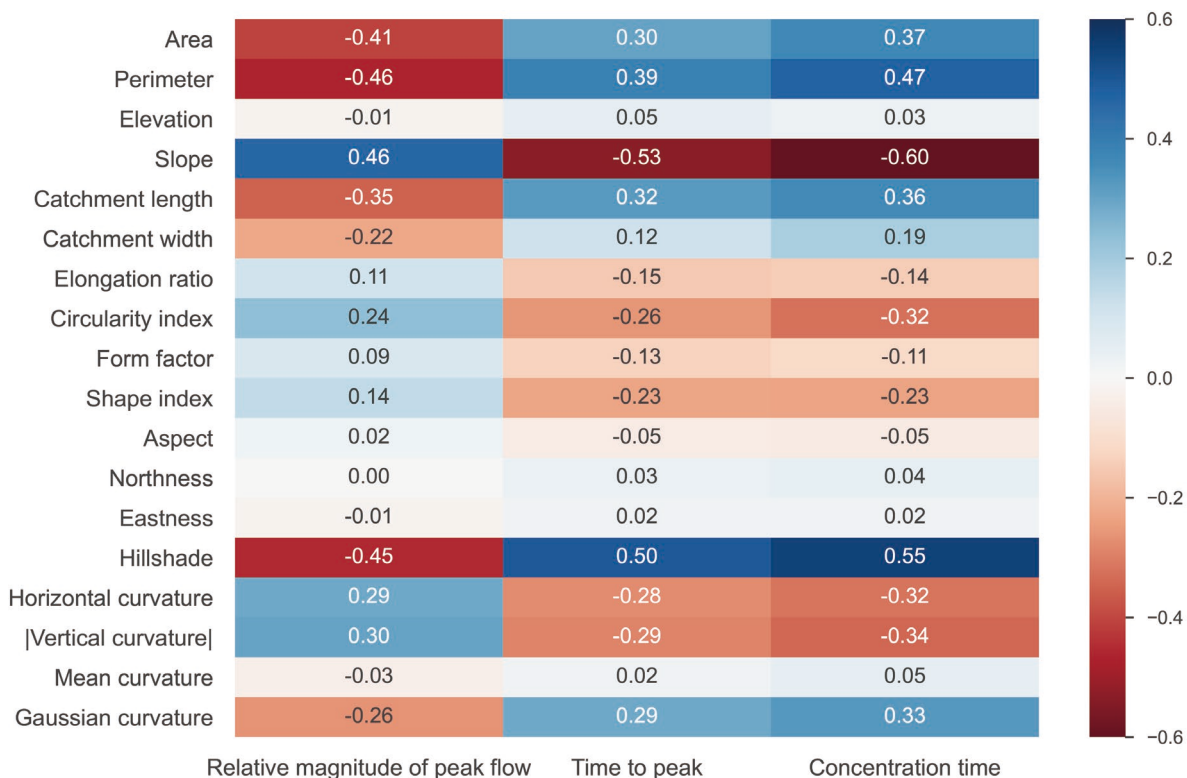
267 hydrograph distribution and a less obvious peak. The higher the  $Q_p$ , the more susceptible the catchment is to flash floods.  
 268 Catchments with a higher  $Q_p$  are found in the northwest or north edge of the Inland Region (IR). Catchments in central IR  
 269 have relatively lower  $Q_p$  due to their smaller slopes. Catchments in the upper Yellow River Basin (YLRB) and Yangtze River  
 270 Basin (YZRB) have correspondingly smaller  $Q_p$  than catchments in lower YLRB and YZRB. Catchments in the Southwest  
 271 Basin (SWB) have the highest  $Q_p$  as compared to catchments in the other three regions. Particularly, in Nu River, Jinsha River,  
 272 Lancang River, and the Palong Zangbo area,  $Q_p$  can reach 0.2 and above, which explains well the high flood risks in those  
 273 regions. In the middle and lower reaches of the Yarlung Zangbo River and the Shiquan River area, the relative magnitude of  
 274 peak flow is also higher than that of the whole Tibetan Plateau.

275 The time to peak time in most catchments mainly ranges from 2h to 15 h, with mean and median  $T_p$  around 10.3h and  
 276 9.0h respectively. The spatial distribution of  $T_p$  across the Tibetan Plateau is similar to that of  $Q_p$ , suggesting the shorter the  
 277  $T_p$ , the higher the  $Q_p$  is. Catchment concentration time however varies from 10h-35h, with mean and median  $T_c$  around 18.3h  
 278 and 16.5h respectively. Catchments with longer  $T_c$  are found in the central TP and YLRB. Catchments in the northwest IR,  
 279 middle and lower reaches of the Yarlung Zangbo River, Palong Zangbo River and the Nu-Jinsha-Lancang basins all have  
 280 relatively short  $T_c$  (<20h). For those regions with high  $Q_p$ , short  $T_p$  and  $T_c$ , it is mainly because the catchments there tend to  
 281 elongate and with a pinnate river network, higher slope and lower roughness.



282  
 283 **Figure 7** Distribution of WFIUH characteristics across the Tibetan Plateau. Left: spatial distribution; right: statistical distribution  
 284 represented by histogram.

285 Figure 8 further shows the relationships of Qp, Tp and Tc against the 18 hydrogeomorphic metrics in our TPHGD dataset.  
 286 It is found that Qp is positively related to slope, horizontal curvature and absolute vertical curvature. Qp is negatively related  
 287 to catchment area, perimeter, length and circularity. The relationships of Tp against the hydrogeomorphic metrics are similar  
 288 to those of Qp but in an opposite direction. This suggests that a catchment with a larger, more circular shape may exhibit a  
 289 more gradual rising limb in its hydrograph. Tc has a strong negative correlation with catchment slope as a steeper land surface  
 290 can result in faster flow hence shortening the travelling time of water flow. Unsurprisingly, Tc is positively related to catchment  
 291 size defined by area, perimeter and length.



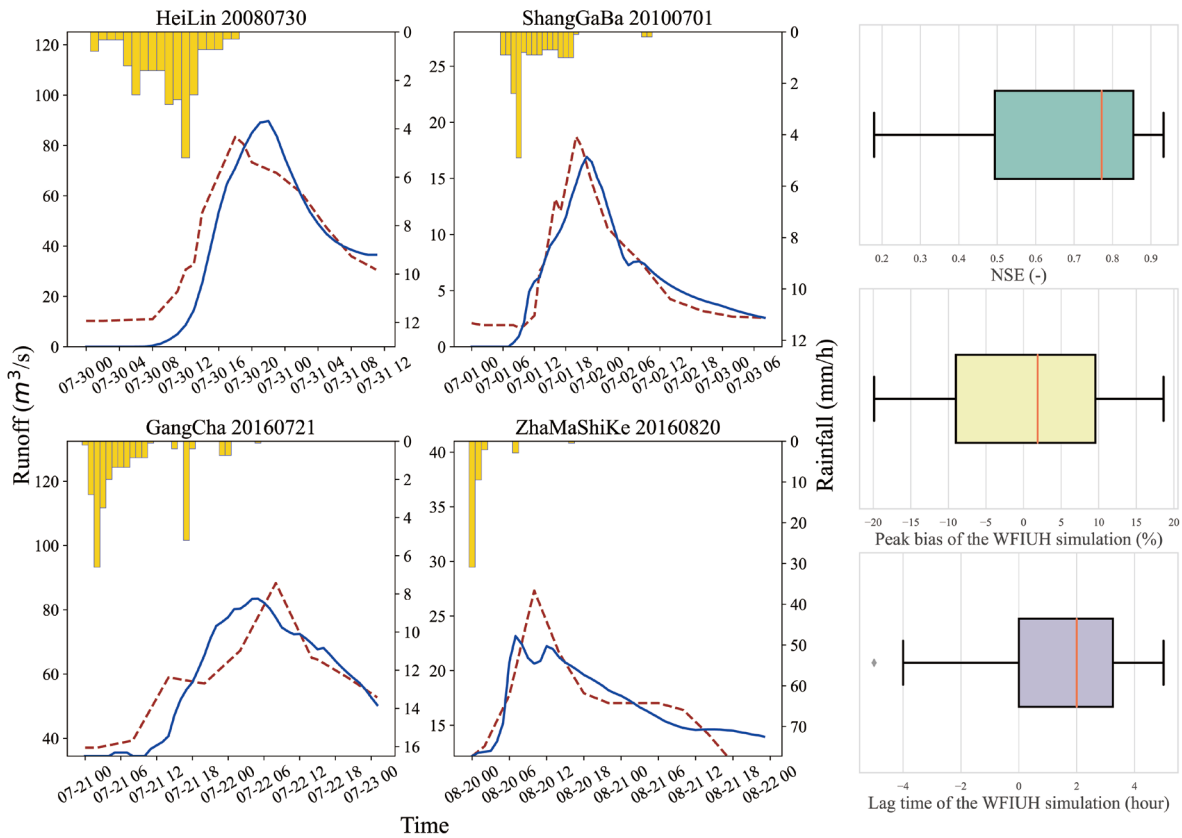
292  
 293 **Figure 8 Correlations between WFIUH characteristics against 18 hydrogeomorphic metrics**

294 **4.4 Validity and uncertainty of derived WFIUH**

295 The derived WFIUH in our TPHGD dataset is expected to represent the hydrological response function in a catchment,  
 296 particularly contributing to generating a hydrograph of ungauged catchments in the Tibetan Plateau. To examine the validity,  
 297 we have incorporated the derived WFIUH into a conceptual hydrological model GR4H (Perrin et al., 2003). The GR4H is a  
 298 model with four parameters running at an hourly time step. The fourth parameter of GR4H (x4) represents the time base of a  
 299 hypothetical unit hydrograph. In this study, the hypothetical unit hydrograph is replaced by our derived WFIUH, and the  
 300 parameter x4 is then removed. The model was tested at four gauged catchments in the Tibetan Plateau for 48 flash flood events

301 from 2008 to 2016. The required inputs of the model (rainfall and potential evapotranspiration) and the observed hourly  
 302 streamflow data are obtained from China's Annual Hydrological Report.

303 Overall, the model performs well for most of the flash flood events as evaluated by NSE (Nash and Sutcliffe, 1970), bias  
 304 in peak flow ( $BS_{qp}$ ) and bias in time to peak ( $BS_{tp}$ ) respectively (Figure 9). The simulated hydrograph is compared to the  
 305 observed one for selected catchments and is shown in Figure 9 as well. As shown in Figure 9, the median NSE of the 48 flash  
 306 events is around 0.67, for more than 50% of the 48 flash flood events with an absolute value of  $BS_{qp}$  lower than 10% and an  
 307 absolute value of  $BS_{tp}$  lower than 3h. Peak flows of 26 flood events are underestimated while that of the other 22 events are  
 308 overestimated, suggesting no systematic tendency in the modelling. The time to peak ( $T_p$ ) of about two-thirds of simulated  
 309 flood events lags behind the observed one, indicating uncertainties in the simulations.



310  
 311 **Figure 9 Performance of hydrological modeling by incorporating WFIUH into GR4H model. Left: comparison between simulated**  
 312 **and observed hydrograph for flash events at different catchments (red-dashed curve is observed, blue-solid curve is simulated);**  
 313 **Right, summary of overall model performance for 48 simulated flash flood events.**

314 Uncertainties of the simulation can not only be due to the uncertainties in the derived WFIUH but also due to uncertainties  
 315 in model structure, model inputs and model parameters. In terms of WFIUH, its validity could be affected by the spatial  
 316 resolution and sources of DEM and the effectiveness of the method in estimating flow velocity. In this study, the DEM dataset  
 317 from SRTM is used, which has with spatial resolution of 90m. We find it challenging to derive WFIUH for catchments with

318 relatively small areas and with highly complicated topography by using the DEM from SRTM. Hence, DEM with higher  
 319 spatial resolution can be conducive to improving the derivation of WFIUG for those catchments. It is worth noting that the  
 320 uncertainties in WFIUH could be considerably affected by the estimate of flow velocity. In this study, Manning’s approach is  
 321 used to calculate flow velocity at each grid cell and then works with the catchment’s width function to derive the WFIUH.  
 322 Other approaches such as the Darcy–Weisbach formula (Katz et al., 1995), the Soil Conservation Service (SCS) formula (Haan  
 323 et al., 1994), and the Maidment et al. (1996) uniform flow equation may result in a different estimate of flow velocity and  
 324 hence the subsequent WFIUH. In addition, the roughness coefficient in Manning’s approach assigned for each grid cell is  
 325 affected by the accuracy of the land cover map, leading to uncertainties in the estimated flow velocity. It has been reported  
 326 that a higher deviation in the roughness coefficient could result in a higher deviation of the hydrograph peaks (Kalyanapu et  
 327 al., 2009). Thus, a detailed evaluation of Manning’s roughness in different land cover types using remote sensing skills is  
 328 needed to reduce the uncertainties (Mtamba et al., 2015; Sadeh et al., 2018). For further exploration of the uncertainties in the  
 329 future, therefore in this version of the dataset, we provide also the width function for each catchment, which facilitates deriving  
 330 WFIUH given different estimates of flow velocity.

## 331 **5 Data and code availability**

332 Our TPHGD dataset provides 18 hydrogeomorphic metrics for 18440 catchments across the Tibetan Plateau, together  
 333 with width function and WFIUH of 13456 out of the 18440 catchments. Table 2 lists the structure of the dataset and the formats  
 334 of the files there. The 18 metrics of all catchments are presented in an Excel file. The catchment’s width function is stored in  
 335 two separate CSV files, one of which represents the distance to the catchment outlet (i.e., x-axis in the WF plot) while the  
 336 other represents the number of cells (equivalent to counts representing y-axis in the WF plot) at a given distance to the outlet.  
 337 The gridded flow velocity map is presented as a tif file in Manning\_velocity\_map. Similar to the catchment’s WF, WFIUH  
 338 for each catchment is presented in two paired CSV files, WFIUH\_flowtime.csv and WFIUH\_cells.csv. The former provides  
 339 flow time at a specific distance to the catchment outlet (i.e., the x-axis in the WFIUH plot), while the latter provides the number  
 340 of cells (equivalent to counts and representing the y-axis in the WFIUH plot) within the corresponding distance. The dataset  
 341 is archived and openly accessible via the Zenodo portal: <https://doi.org/10.5281/zenodo.8280786> (Guo and Zheng, 2023).

342 The Python scripts in deriving WFIUH, curve fitting, and classification are freely available at  
 343 [https://github.com/YuhanGuo-22/Hydro\\_WFIUH\\_Classifier\\_and\\_Curve\\_fitting.git](https://github.com/YuhanGuo-22/Hydro_WFIUH_Classifier_and_Curve_fitting.git) (last access: 18 Oct 2023). The  
 344 dependency Python package (pysheds) used in deriving catchment WF is available at <https://github.com/mdbartos/pysheds>.

345

346 **Table 2 Files in the TPHGD dataset**

File names	Formats	Descriptions
1-Hydro_geomorphic_attribute	.xlsx 18440× 26	

		Hydrogeomorphic metrics of 18440 catchments. Each row represents one catchment. Each column represents one metric (see Table 1).
2-WF_distance	.csv 13456 columns	Catchments' width function: distance to outlet (WF's x-axis). The first row is the catchment ID. Each column represents the distance to the catchment outlet for a catchment.
2-WF_cells.csv	.csv 13456 columns	Catchments' width function: cells/area (WF's y-axis). The first row is the catchment ID. Each column represents cells between a specific distance and an outlet for a catchment.
3-Manning_velocity_map	.tif (90m resolution)	Gridded flow velocity was calculated by Manning's approach. The value of each grid represents the mean velocity along the shortest flow path to the outlet.
4-WFIUH_flowTime.csv	.csv 13456 columns	Catchments' WFIUH: flow time to the outlet (WFIUH's x-axis). The first row is the catchment ID. Each column represents flow time to the outlet for a catchment.
4-WFIUH_cells.csv	.csv 13456 columns	Catchments' WFIUH: cells/area to outlet corresponding to a specific flow time (WFIUH's y-axis). The first row is the catchment ID. Each column represents the number of cells with a specific flow time to the outlet of a catchment.

347

## 348 6 Conclusions

349 The Tibetan Plateau provides an ideal setting for investigating the hydrological and geomorphic interactions between  
350 hydrological and geomorphic processes in a largely pristine natural environment, minimally impacted by human activities.  
351 The hydrological behaviours of catchments across the Tibetan Plateau however remain largely unknown due to its challenging  
352 physical conditions and data limitations. This study presents the inaugural version of a hydrogeomorphic dataset encompassing  
353 18,440 catchments across the region. The dataset comprises 18 hydrogeomorphic metrics, particularly along with the width  
354 function and width function-based instantaneous unit hydrograph of each catchment. It can contribute to advancing our  
355 understanding of catchment hydrological behaviors in the Tibetan Plateau and hence improving water resources management  
356 and disaster mitigation in the region and its downstream. Particularly, the newly derived WFIUH can be conducive to flash  
357 flood modeling in catchments with little hydrological observations.

358 According to the dataset provided, it is found that catchments with higher elevation are in the western and central parts  
359 of the TP, while catchments in the western and southeast TP are steeper than other catchments in the TP. Catchments in central  
360 TP are more elongated with the pinnate river network, and catchments in western and eastern TP are less elongated and more  
361 fan-shaped. A power relationship (i.e., Hack's law) exists between catchments' area and length. We also find that the peak  
362 flow of WFIUH is positively related to slope and curvature but negatively related to catchment area, perimeter, length and  
363 circularity. The relationships of time-to-peak against the hydrogeomorphic metrics are similar to those of peak flow but in an  
364 opposite direction. Catchment concentration time shows a positive relationship with catchment size but a strong negative

365 correlation with catchment slope as a steeper land surface can result in faster flow hence shortening the travelling time of water  
366 flow.

367 The validity of the derived WFIUH has been confirmed by its successful integration into an hourly hydrological model for  
368 simulating flash flood events. Uncertainties in the simulation may arise from factors such as model structure, model inputs,  
369 model parameterization, and the derived WFIUH. Particularly, uncertainties in the WFIUH can be attributed to the resolution  
370 of DEM and the methods employed for calculating flow velocity. These aspects warrant further exploration in future research  
371 endeavors.

#### 372 **Author contributions.**

373 HZ, YS, YY and YG conceived the research. YG and HZ developed the approaches and datasets. YY and YS checked the  
374 results. YG and HZ wrote the original draft. YY, YS and CW revised the draft.

375

#### 376 **Competing interests.**

377 The contact author has declared that none of the authors has any competing interests.

## 378 **References**

- 379 Babar, M.: Hydrogeomorphology: fundamentals, applications and techniques, 2005.  
380 Bhaskar, N. R., Parida, B. P., and Nayak, A. K.: Flood estimation for ungauged catchments using the GIUH, Journal of water resources  
381 planning management, 123, 228-238, 1997.  
382 Botter, G. and Rinaldo, A.: Scale effect on geomorphologic and kinematic dispersion, Water Resources Research, 39, 2003.  
383 Esper Angillieri, M. Y.: Morphometric analysis of Colangüil river basin and flash flood hazard, San Juan, Argentina, Environmental geology,  
384 55, 107-111, 2008.  
385 Florinsky, I.: Digital terrain analysis in soil science and geology, Academic Press 2016.  
386 Franchini, M. and O'Connell, P. E.: An analysis of the dynamic component of the geomorphologic instantaneous unit hydrograph, Journal  
387 of Hydrology, 175, 407-428, 1996.  
388 Franchini, M. and O'Connell, P. E.: An analysis of the dynamic component of the geomorphologic instantaneous unit hydrograph, Journal of  
389 Hydrology, 175, 407-428, 10.1016/S0022-1694(96)80018-7, 1996.  
390 Ge, J., You, Q., and Zhang, Y.: Effect of Tibetan Plateau heating on summer extreme precipitation in eastern China, Atmospheric Research,  
391 218, 364-371, 2019.  
392 Grimaldi, S., Petroselli, A., Alonso, G., and Nardi, F.: Flow time estimation with spatially variable hillslope velocity in ungauged basins,  
393 Advances in Water Resources, 33, 1216-1223, 10.1016/j.advwatres.2010.06.003, 2010.  
394 Guo, Y. and Zheng, H.: Hydro-geomorphic unit hydrograph dataset of catchments across the Tibetan Plateau, Zenodo [data set],  
395 <https://doi.org/10.5281/zenodo.8280786>, 2023.  
396 Gupta, V. K. and Waymire, E.: On the formulation of an analytical approach to hydrologic response and similarity at the basin scale, Journal  
397 of Hydrology, 65, 95-123, 1983.  
398 Gupta, V. K., Waymire, E., and Wang, C.: A representation of an instantaneous unit hydrograph from geomorphology, Water resources  
399 research, 16, 855-862, 1980.  
400 Haan, C. T., Barfield, B. J., and Hayes, J. C.: Design hydrology and sedimentology for small catchments, Elsevier 1994.  
401 Horton, R. E.: Erosional development of streams and their drainage basins-Hydrophysical approach to quantitative morphology, Bull. G. S.  
402 A, 56, 1945.  
403 Jain, S., Singh, R., and Seth, S.: Design flood estimation using GIS supported GIUH Approach, Water resources management, 14, 369-376,  
404 2000.  
405 Jenson, S. K.: Applications of hydrologic information automatically extracted from digital elevation models, Hydrol. Process., 5, 31-44,  
406 1991.  
407 Kalyanapu, A. J., Burian, S. J., and McPherson, T. N.: Effect of land use-based surface roughness on hydrologic model output, Journal of  
408 Spatial Hydrology, 9, 2009.  
409 Kang, S., Xu, Y., You, Q., Flügel, W.-A., Pepin, N., and Yao, T.: Review of climate and cryospheric change in the Tibetan Plateau,  
410 Environmental research letters, 5, 015101, 2010.

411 Katz, D. M., Watts, F. J., and Burroughs, E. R.: Effects of surface roughness and rainfall impact on overland flow, *Journal of Hydraulic*  
412 *Engineering*, 121, 546-553, 1995.

413 Kirkby, M.: Tests of the random network model, and its application to basin hydrology, *Earth Surface Processes*, 1, 197-212, 1976.

414 Kirshen, D. M. and Bras, R. L.: The linear channel and its effect on the geomorphologic IUH, *Journal of Hydrology*, 65, 175-208, 1983.

415 Koenderink, J. J. and Van Doorn, A. J.: Surface shape and curvature scales, *Image vision computing*, 10, 557-564, 1992.

416 Kumar, R., Chatterjee, C., Singh, R., Lohani, A., and Kumar, S.: Runoff estimation for an ungauged catchment using geomorphological  
417 instantaneous unit hydrograph (GIUH) models, *Hydrological Processes: An International Journal*, 21, 1829-1840, 2007.

418 Lehner, B., Verdin, K., and Jarvis, A.: New Global Hydrography Derived From Spaceborne Elevation Data, *Eos, Transactions American*  
419 *Geophysical Union*, 89, 93, 10.1029/2008eo100001, 2008.

420 Li, X., Long, D., Scanlon, B. R., Mann, M. E., Li, X., Tian, F., Sun, Z., and Wang, G.: Climate change threatens terrestrial water storage  
421 over the Tibetan Plateau, *Nature Climate Change*, 12, 801-807, 10.1038/s41558-022-01443-0, 2022.

422 Lindersson, S., Brandimarte, L., Mård, J., and Di Baldassarre, G.: Global riverine flood risk—how do hydrogeomorphic floodplain maps  
423 compare to flood hazard maps?, *Natural hazards earth system sciences*, 21, 2921-2948, 2021.

424 Maidment, D., Olivera, F., Calver, A., Eatherall, A., and Fraczek, W.: Unit hydrograph derived from a spatially distributed velocity field,  
425 *Hydrol. Process.*, 10, 831-844, 1996.

426 Mesa, O. J. and Mifflin, E. R.: On the relative role of hillslope and network geometry in hydrologic response, in: *Scale problems in hydrology*,  
427 Springer, 1-17, 1986.

428 Mölg, T., Maussion, F., and Scherer, D.: Mid-latitude westerlies as a driver of glacier variability in monsoonal High Asia, *Nature Climate*  
429 *Change*, 4, 68-73, 10.1038/nclimate2055, 2014.

430 Moussa, R.: What controls the width function shape, and can it be used for channel network comparison and regionalization?, *Water*  
431 *Resources Research*, 44, 19, 10.1029/2007wr006118, 2008.

432 Mtamba, J., Van Der Velde, R., Ndomba, P., Zoltán, V., and Mtalo, F.: Use of Radarsat-2 and Landsat TM Images for Spatial  
433 Parameterization of Manning's Roughness Coefficient in Hydraulic Modeling, *Remote Sensing*, 7, 836-864, 10.3390/rs70100836, 2015.

434 NADEN, P. S.: Spatial variability in flood estimation for large catchments: the exploitation of channel network structure, *Hydrological*  
435 *Sciences Journal*, 37, 53-71, 1992.

436 Nash, J. E. and Sutcliffe, J. V.: River flow forecasting through conceptual models part I—A discussion of principles, *Journal of Hydrology*,  
437 10, 282-290, 1970.

438 Nasri, S., Cudennec, C., Albergel, J., and Berndtsson, R.: Use of a geomorphological transfer function to model design floods in small  
439 hillside catchments in semiarid Tunisia, *Journal of hydrology*, 287, 197-213, 2004.

440 Nowicka, B. and Soczynska, U.: Application of GIUH and dimensionless hydrograph models in ungauged basins, *FRIENDS in Hydrology*,  
441 187, 197-203, 1989.

442 Passalacqua, P., Tarolli, P., and Foufoula-Georgiou, E.: Testing space-scale methodologies for automatic geomorphic feature extraction from  
443 lidar in a complex mountainous landscape, *Water resources research*, 46, 2010.

444 Peng Gong, Han Liu, Meinan Zhang, Li, C., Wang, J., and Huang, H.: Stable classification with limited sample: Transferring a 30-m  
445 resolution sample set collected in 2015 to mapping 10-m resolution global land cover in 2017, *Sci. Bull.*, 64, 370-373, 2019.

446 Perrin, C., Michel, C., and Andréassian, V.: Improvement of a parsimonious model for streamflow simulation, *Journal of hydrology*, 279,  
447 275-289, 2003.

448 Prusevich, A., Lammers, R., and Glidden, S.: MERIT-Plus Dataset: Delineation of endorheic basins in 5 and 15 min upscaled river networks,  
449 *MultiSector Dynamics-Living, Intuitive, Value-adding, Environment*, 2022.

450 Rigon, R., Rodriguez-Iturbe, I., Maritan, A., Giacometti, A., Tarboton, D. G., and Rinaldo, A.: On Hack's Law, *Water Resources Research*,  
451 32, 3367-3374, 10.1029/96wr02397, 1996.

452 Rinaldo, A., Marani, A., and Rigon, R.: Geomorphological dispersion, *Water Resources Research*, 27, 513-525, 1991.

453 Rinaldo, A., Vogel, G. K., Rigon, R., and Rodriguez-Iturbe, I.: Can one gauge the shape of a basin, *Water Resources Research*, 31, 1119-  
454 1127, 10.1029/94wr03290, 1995.

455 Rodríguez-Iturbe, I. and Valdes, J. B.: The geomorphologic structure of hydrologic response, *Water resources research*, 15, 1409-1420, 1979.

456 Rodríguez-Iturbe, I. and Valdés, J. B.: The geomorphologic structure of hydrologic response, *Water resources research*, 15, 1409-1420, 1979.

457 Saco, P. M. and Kumar, P.: Kinematic dispersion effects of hillslope velocities, *Water Resources Research*, 40, n/a-n/a,  
458 10.1029/2003wr002024, 2004.

459 Sadeh, Y., Cohen, H., Maman, S., and Blumberg, D.: Evaluation of Manning's n Roughness Coefficient in Arid Environments by Using  
460 SAR Backscatter, *Remote Sensing*, 10, 1505, 10.3390/rs10101505, 2018.

461 Safanelli, J., Poppiel, R., Ruiz, L., Bonfatti, B., Mello, F., Rizzo, R., and Demattê, J.: Terrain Analysis in Google Earth Engine: A Method  
462 Adapted for High-Performance Global-Scale Analysis, *ISPRS International Journal of Geo-Information*, 9, 400, 10.3390/ijgi9060400, 2020.

463 Sassolas-Serrayet, T., Cattin, R., and Ferry, M.: The shape of watersheds, *Nature Communications*, 9, 10.1038/s41467-018-06210-4, 2018.

464 Scheidegger, A. E.: Hydrogeomorphology, *Journal of Hydrology*, 20, 193-215, 1973.

465 Sidle, R. C. and Onda, Y.: Hydrogeomorphology: overview of an emerging science, *Hydrol. Process.*, 18, 597-602, 2004.

466 Singh, P., Mishra, S., and Jain, M.: A review of the synthetic unit hydrograph: from the empirical UH to advanced geomorphological methods,  
467 Hydrological Sciences Journal, 59, 239-261, 2014.  
468 Strahler, A. N.: Quantitative analysis of watershed geomorphology, Eos, Transactions American Geophysical Union, 38, 913-920, 1957.  
469 Troutman, B. M. and Karlinger, M. R.: Unit hydrograph approximations assuming linear flow through topologically random channel  
470 networks, Water Resources Research, 21, 743-754, 10.1029/wr021i005p00743, 1985.  
471 Yang, L., Ma, J., Wang, X., and Tian, F.: Hydroclimatology and Hydrometeorology of Flooding Over the Eastern Tibetan Plateau, Journal  
472 of Geophysical Research: Atmospheres, 127, e2022JD037097, 2022.  
473 Yao, T., Thompson, L., Yang, W., Yu, W., Gao, Y., Guo, X., Yang, X., Duan, K., Zhao, H., Xu, B., Pu, J., Lu, A., Xiang, Y., Kattel, D. B.,  
474 and Joswiak, D.: Different glacier status with atmospheric circulations in Tibetan Plateau and surroundings, Nature Climate Change, 2, 663-  
475 667, 10.1038/nclimate1580, 2012.  
476 Yao, T., Bolch, T., Chen, D., Gao, J., Immerzeel, W., Piao, S., Su, F., Thompson, L., Wada, Y., Wang, L., Wang, T., Wu, G., Xu, B., Yang,  
477 W., Zhang, G., and Zhao, P.: The imbalance of the Asian water tower, Nature Reviews Earth & Environment, 10.1038/s43017-022-00299-  
478 4, 2022.  
479